Available online at www.sciencedirect.com
SCIENCE DIRECT
Polymer 47 (2006) 1267–1280
polymer
www.elsevier.com/locate/polymer

Thermo-mechanical properties of LLDPE/SiO_2 nanocomposites

E. Kontou *, M. Niaounakis

Department of Applied Mathematical and Physical Sciences Section of Mechanics, National Technical University of Athens, 5 Heroes of Polytechnion, GR-15773 Athens, Greece

Received 19 October 2005; received in revised form 11 December 2005; accepted 12 December 2005
Available online 10 January 2006

Abstract

Two series of linear low density polyethylene (LLDPE)/SiO_2 nanocomposites were prepared. They were based on two types of commercial LLDPE, one prepared by metallocene (mLLDPE) and the other by traditional Ziegler–Natta (zLLDPE) catalysts, and silica nanoparticles surface treated with dimethyldichlorosilane. The silica nanonparticles used have an average diameter of 16 nm, and their weight fraction varied from 2 up to 10%. The structure and thermal-mechanical features of the nanocomposites were characterized by scanning electron microscopy (SEM), differential scanning calorimetry (DSC), dynamic mechanical spectroscopy (DMA) as well as tensile tests. The effect of nanoparticles on crystallinity, and hence to the morphology of the materials was studied. The secondary transitions were also affected by the filler presence, while the tensile properties were reinforced with varying the nanoparticle weight fraction. The addition of the nanofillers brought up an increase in the elastic modulus and the tensile strength of mLLDPE accompanied by an unusual dramatic increase in the elongation at break. The same trend, although to a lesser extent, was observed for the zLLDPE/SiO_2 composites. The increment of the elastic modulus of the composites with increasing filler content was simulated with three micromechanical models developed in previous works. The model which assumes an effective interface between the matrix and the nanoparticles provided the best fitting with the experimental data of mLLDPE/SiO_2.

Keywords: LLDPE; Nanocomposites; Silica

1. Introduction

Polyethylene, with one third of the world plastic production, is one of the most versatile polymers, mainly due to its low density, good processability and low cost. However, its use is restricted because of several drawbacks, including lower strength and poor heat resistance. To overcome these drawbacks and to prepare materials with enhanced properties, in the past years polyethylene nanocomposites with several inorganic nanofilllers were prepared [1–13]. An attractive feature of polymer nanocomposites is the promise of significantly improved stiffness and tensile strength, for a minor increase in specific gravity over the unmodified polymer. One of the few disadvantages associated with the use of nanofillers is their high cost. However, this negative effect of high cost is counterbalanced as only relatively small amounts (2–5%) of nanofillers are needed, while traditional fillers require a much higher loading to achieve a similar performance.

The nanosize fillers can be generally any filler or combination of fillers having at least one dimension (length, width, or thickness) from about 1 to about 30 nm. When only one dimension is in the nanometer range, the filler is present in the form of sheets of one to a few nanometers thick to hundreds or thousands nanometers long, such as platelet clays and layered silicates (phylosilicates). When the two dimensions are in the nanometer scale and the third is larger, the filler forms an elongated structure, for example carbon nanotubes or cellulose whiskers. When the three dimensions are in the order of nanometers, the filler is present in the form of spherical nanoparticles, such as silicas or zeolites, or even can include semiconductory nanoclusters [14].

Despite the efforts that have been directed towards the preparation of polymer nanocomposites and the unique properties of these materials, there are quite enough aspects, associated with their structure and mechanisms of reinforcement that remain unclear [15]. In mechanical reinforcement major issues are the homogeneous dispersion of nanofillers in the polymeric matrix and the development of chemical bonding or strong interactions at the nanofiller–matrix

* Corresponding author. Tel.: +30 210 7721219; fax: +30 210 7721302.
E-mail address: ekontou@central.ntua.gr (E. Kontou).

0032-3861/$ - see front matter © 2005 Elsevier Ltd. All rights reserved.
doi:10.1016/j.polymer.2005.12.039

interface. Regarding polyethylene, the dispersion quality of inorganic nanofillers is one of the main difficulties. This is due to the hydrophobic nature of polyethylene, which gives rise to a significant problem in enhancing adhesion between the 'hydrophilic' nanofiller and the matrix creating poor bond strength between the polymer matrix and filler. The problem of poor dispersibilty of nanofillers in a polyethylene matrix can be solved by a number of techniques including in situ polymerization of monomers in the presence of nanoparticles (e.g. sol–gel process [1,2] and intercalation polymerization [3,4]), use of compatibilizers [5,6], modification of the nanoparticles with coupling agents (e.g. silane coupling) [7–9], or through graft polymerization [10]. Although most of these techniques provide satisfactory dispersion of the nanoparticles, they are, nevertheless characterized by complex polymerization and processing conditions, which add to the already high cost of the nanoparticles [14]. In addition, most of the nanoparticles are non-layered inorganic substances.

Taking into account the above consideration in combination with the availability of processing methods, it can be concluded that the conventional compounding techniques used for the preparation of microcomposites are still the most convenient candidates for the preparation of nanocomposites. In the case of melt compounding since the filler dispersion is poor a coupling agent is used [7–9]. The surface treatment of the nanofiller by a coupling agent improves the degree of wetting of the nanofiller by the polymer and its dispersion in the polymer matrix. However, the modification of the nanofillers by a coupling agent is restricted by the tendency of the nanoparticles to form agglomerates which prevent the coupling agent to penetrate into the agglomerated nanoparticles easily and react with the activated sites of the nanoparticles.

Most of polyethylene is used in film applications. Commercial film-forming polyethylenes comprise low-density polyethylene (LDPE) and linear low-density polyethylene (LLDPE). LLDPE is used extensively as packaging film due to its excellent mechanical properties, such as tear and impact strength as well as high tensile strength. LLDPE is a copolymer of ethylene and an a-olefin or diene, such as butene, hexene and octene. LLDPE consists of a linear backbone structure with little or no long chain branching as opposed to LDPE, which has a significant inclusion of long chain branches. However, despite all its attributes, LLDPE is not an ideal material even for films, where it is most commonly used. LLDPEs polymerized by Ziegler–Natta catalysts (zLLDPE) contain a significant low molecular weight, *n*-hexane extractable constituent and they yield films which have low clarity and low gloss. LDPEs polymerized by metallocene catalysts (mLLDPE) have several advantages over zLLDPE, such as strength, optical properties, narrow molecular weight distribution and low extractables, but are more difficult to process into films [16]. In general, the incorporation of fillers in LLDPE increases the elastic modulus of the material and can increase its tensile strength, but it almost invariably decreases the elongation at break [11].

Several models have been proposed for the prediction of the elastic modulus of composites, but the fundamental mechanisms for mechanical enhancement of polymer nanocomposites are not yet completely defined [11,17,18].

Most of the models have been developed for microcomposites and, as a matter of fact, they do not describe satisfactorily the experimental behavior of nanocomposites. The main reasons for the high deviation between experimental and theoretical results are: (i) all the models assume a perfect adhesion between the filler and matrix; this is not necessarily true in the case of surface treated fillers; (ii) the very large surface area of the nanofillers which can affect the nature and extent of the interphase.

In the present work, two series of LLDPE/SiO_2 nanocomposites were prepared and studied experimentally using scanning electron microscopy (SEM), differential scanning calorimetry (DSC), dynamic mechanical spectroscopy (DMA) and tensile testing. Two types of commercial LLDPE were used, one prepared by Ziegler–Natta (zLLDPE) and the other by metallocene catalysts (mLLDPE). The different morphology of the LLDPE matrices was found to affect the thermo-mechanical behavior of the nanocomposites examined. Moreover, the degree of enhancement, expressed by the elastic modulus, normalized in respect to the pure matrix modulus, was described by three micromechanical models developed in the literature. It was found that due to the different matrix morphology, different assumptions should be made for the modeling of the modulus of the nanocomposites studied. The interphase was found to play a major role in nanocomposites.

2. Materials

Two types of LLDPE were used as matrix materials for the polyolefin nanocomposites under investigation. The first type is based on octene comonomer, prepared by metallocene catalyst designated as mLLDPE, and the other type based on butene comonomer, was prepared by Ziegler–Natta catalyst (zLLDPE). The characteristics of the matrix polymers supplied by Flexopack SA, Athens, Greece, are presented in Table 1. The density of pellets was measured in an isopropanol-distilled water gradient column, calibrated with glass floats. The melt flow index (MFI) was measured at 190 °C at a load of 2.16 kg, according to ASTM-D1238-65T.

Silica Aerosil R972 (supplied by Degussa Chemicals) was used for the preparation of the nanocomposites. Aerosil R972 is a hydrophobic fumed silica after treated with DDS

Table 1
Characteristics of the LLDPE polymers

Material	Density (g/cm^3)	MFI (g/10 min)	Comonomer type	Comonomer content (%)
LLDPE	0.902	1.00	C_8	15
LLDPE	0.924	1.02	C_4	5.5

(dimethyldichlorosilane) based on a hydrophilic fumed silica, with a specific surface area of 130 m^2/g. The average primary particle size is 16 nm.

Five percentage contents of silica were studied namely 2, 4, 6, 8 and 10% per weight. The pure matrix was also studied. Mixing of Aerosil silica with the LLDPE materials was performed with a Brabender mixer. The temperature was 170 °C and the rotation speed of the screws was 40 rpm. The silica powder was fed to the polymer melt slowly to achieve the optimum particle dispersion. Hereafter, the materials were compression molded at 130 °C, using a thermo-press and a special mould of 2 mm thickness.

3. Experimental

Scanning electron microscopy (SEM) images were obtained using a JEOL 6300 scanning microscope operated at an acceleration voltage of 20 kV and equipped with an energy-dispersive system (EDS). All the studied samples were coated with carbon black to avoid charging under the electron beam.

Calorimetric measurements were carried out using a Setaram DSC 141 instrument, with a pulsed nitrogen cooling system. The instrument was calibrated with an Indium standard. All materials were treated in the same way: they were heated with a constant heating rate of 40 °C/min from ambient temperature up to 160 °C, to erase previous history, They were held for 2 min at 160 °C, subsequently cooled down to −100 °C, and after an isothermal hold of 2 min, the samples were heated at a rate of 10 °C/min up to 160 °C, and the corresponding thermogram was recorded. Calculations of the percent crystallinity were based on a heat of fusion of 290 J/g for the perfect crystal [19]. The glass transition temperature, T_g, was measured as the inflection point of the heating curve and the melting temperature, T_m was taken as the maximum in the transition endotherm. The non-isothermal crystallization measurements were carried out from the melt at 160 °C with a cooling rate of 20 °C down to −100 °C.

DMA experiments were performed using the Perkin–Elmer DMA 7e instrument. The mode of deformation applied was the three-point bending system, and the mean dimensions of sample plaques were 2 mm × 4 mm × 20 mm. The temperature range varied from −170 °C up to the melting temperature of the materials. The temperature dependent behavior was studied by monitoring changes in force and phase angle, keeping the amplitude of oscillation constant. The frequency was 1 Hz and the heating rate 5 °C/min. The storage and loss moduli curves versus temperature were evaluated.

Tensile measurements were carried out with an Instron 1121 type tester, at room temperature. The dumbbell type specimens were of a gauge length of 30 mm, and the applied crosshead

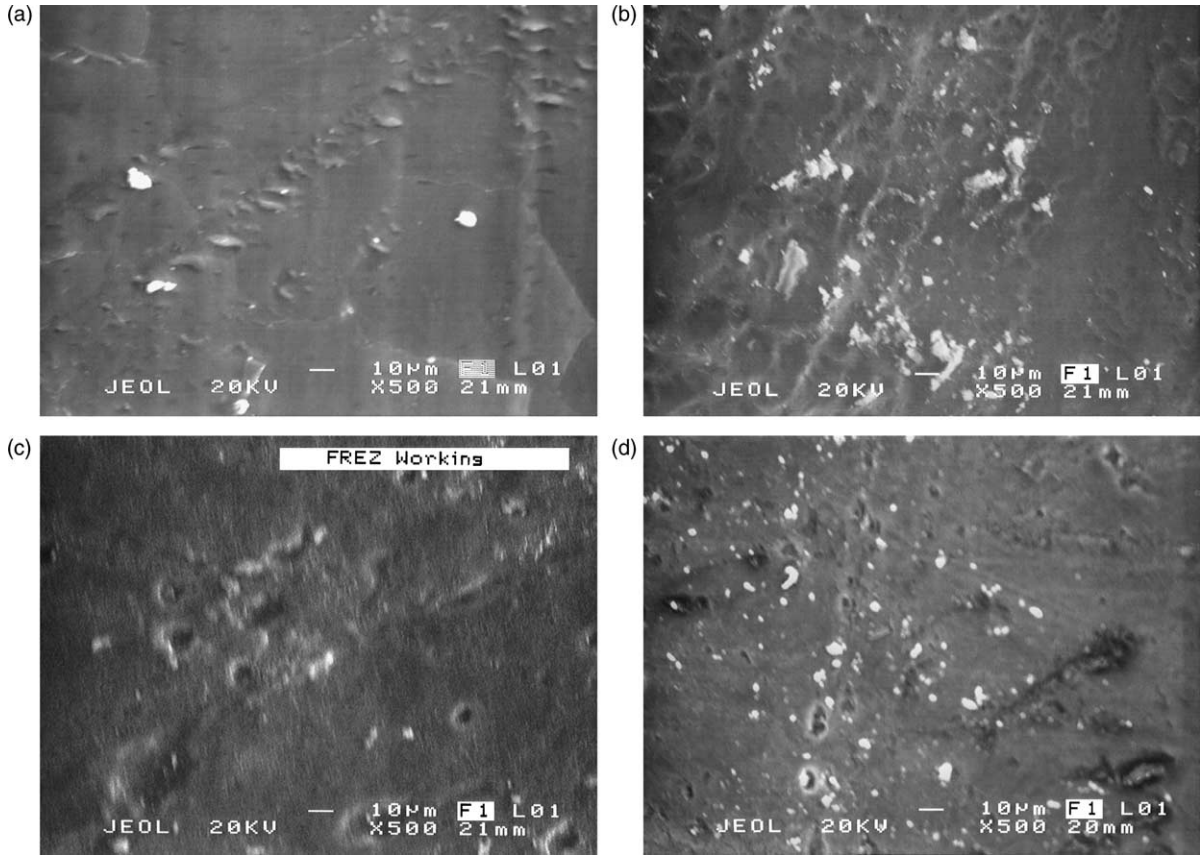

Fig. 1. (a) SEM micrographs of the mLLDPE/SiO_2 nanocomposites with a silica content of 4% per weight. (b) SEM micrographs of the mLLDPE/SiO_2 nanocomposites with a silica content of 8% per weight. (c) SEM micrographs of the zLLDPE/SiO_2 nanocomposites with a silica content of 4% per weight. (d) SEM micrographs of the zLLDPE/SiO_2 nanocomposites with a silica content of 8% per weight.

speed was 10 mm/min. This value corresponds to an effective strain rate of 5.55×10^{-3} s^{-1}. Engineering tensile stress–strain curves were then obtained up to the breaking point.

4. Results and discussion

4.1. SEM results

Fig. 1(a)–(d) shows the SEM micrographs of mLLDPE/SiO_2 and zLLDPE/SiO_2 composites, respectively, with a silica content of 4 and 8%. The study of the SEM images revealed that all the samples contain agglomerates the size of which varied with the silica content. For a silica content of 4%, the mLLDPE-based composite exhibited agglomerates with a particle size of less than 600 nm and a few large agglomerates in the size range of 5–10 μm. At a silica content of 8%, the number of large agglomerates increased substantially while some of them exceeded the size of 10 μm. Compared with the corresponding zLLDPE/SiO_2 nanocomposites, the size of agglomerates are smaller. These results are also in good agreement with the findings of Wu et al. [20] and Bikiaris et al. [21], who reported that increasing the silica content in polypropylene nanocomposites leads to larger agglomerates.

At this point is worth noting that the market available nanoparticles generally take the form of agglomerates, which are hard to be broken apart during compounding due to the strong interaction among the nanoparticles, the limited shear force provided by the mixing device and the high melt viscosity of polymer melts. Modification of the nanoparticles with a coupling agent, as in the present case, is restricted by the inability of the coupling agent to penetrate into the agglomerated nanoparticles easily and react with the activated sites of the nanoparticles. Based on these facts, we can infer that it might be impossible to pursue an efficient nanoscale dispersion of the silica particles, especially when considering the high viscosity of the LLDPE melt (MFI about 1 g/10 min). Although there are several methods available for an efficient nanoscale dispersion, most of them are either not applicable to most of the technically important polymers or they are not cost effective. Taking into account the above consideration, it can be concluded that the conventional compounding techniques used for the preparation of microcomposites are still the most convenient candidates for the preparation of nanocomposites.

Furthermore, the scope of the present study was to find the optimum silica content (surface treated silica Aerosil) for the two types of LLDPE-base composites by using the conventional compounding techniques for the preparation of microscale filled polymers.

4.2. DSC results

The heating thermograms of the mLLDPE/SiO_2 and zLLDPE/SiO_2 composites are presented in Figs. 2 and 3, respectively. The DSC results in terms of glass transition temperature (T_g), melting temperature (T_m), heat of fusion (ΔH), and the percentage crystallinity (x_c) are summarized in Tables 2 and 3, respectively. The corresponding cooling thermograms of the non-isothermal crystallization are presented in Figs. 4 and 5.

The T_g of mLLDPE (−40 °C) was higher than that of zLLDPE (−50 °C). This is attributed to the higher comonomer content (15%), which in combination with the uniform distribution of short branches leads to a reduced chain flexibility and consequently to an elevated T_g. The T_gs of the LLDPE/SiO_2 composites were higher compared to the T_g of the corresponding LLDPE due to the restriction of silica nanoparticles on the segmental and long-range chain mobility of the LLDPE phase. However, no trend was established between Tg and silica content.

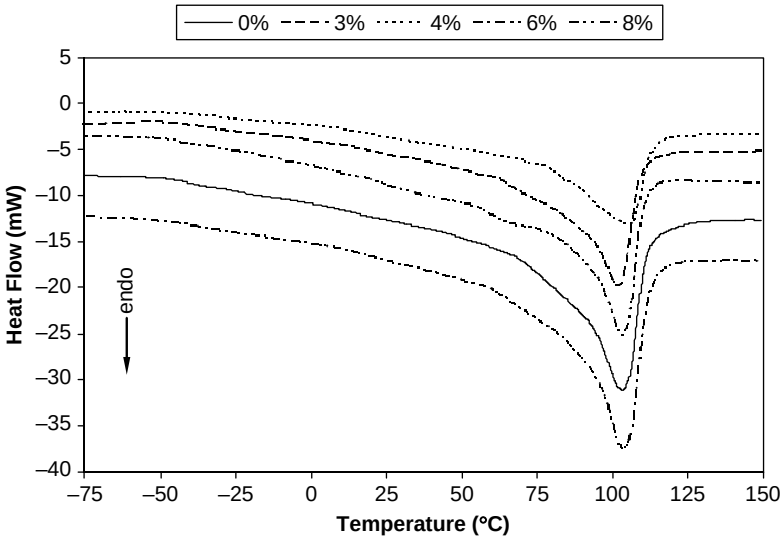

Fig. 2. DSC thermograms of the mLLDPE/SiO_2 nanocomposites at a heating rate of 10 °C/min. The curves have been shifted in the y-direction to make them distinguishable.

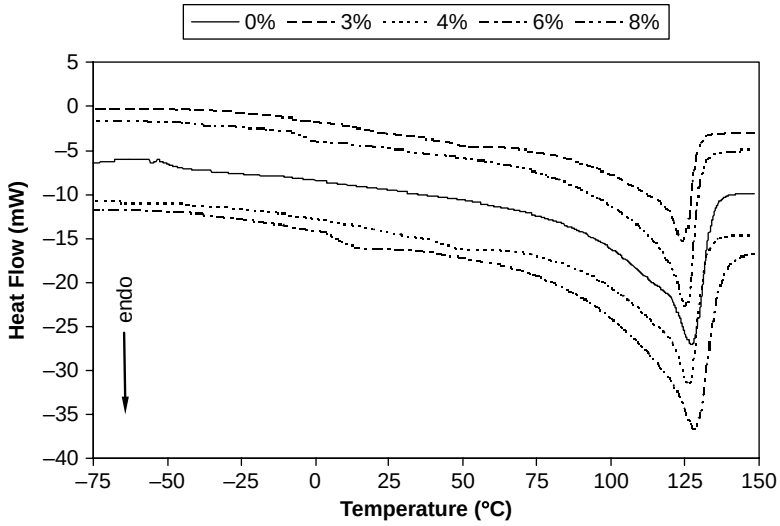

Fig. 3. DSC thermograms of the zLLDPE/SiO_2 nanocomposites at a heating rate of 10 °C/min. The curves have been shifted in the *y*-direction to make them distinguishable.

Regarding the melting behavior of the pure materials, zLLDPE exhibits a much higher melting temperature (127 °C) than mLLDPE (103 °C). Furthermore, the DSC measurements show that the melting peak of both types of composites is not significantly affected by changes in the silica content. Moreover, the melt enthalpy of mLLDPE/SiO_2 increased up to a silica content of 4% and then decreased. A similar, although less pronounced, trend was observed for the zLLDPE/SiO_2 composites.

As far as the zLLDPE/SiO_2 composites are concerned, the addition of the silica nanofillers is considered to be responsible for the appearance of an intense shoulder in the temperature range from 25 to 75 °C which is shifted to lower temperatures with increase in the silica content. The mLLDPE/SiO_2 composites did not show any distinct paracrystalline region. Only a weak shoulder could be seen in the low temperature side of the melting curve as result of the addition of silica.

The melting behavior of LLDPE/SiO_2 composites can be explained as follows: the difference in melting temperatures of the pure materials is attributed mainly to differences in the comonomer content of the LLDPEs and the polymerization catalysis. The higher co-monomer content of mLLDPE (15%) provides a larger number of short chain branches homogeneously distributed along the polymer chains of mLLDPE, which hinder the crystallization of the linear parts, and contribute to the lowering of the melting temperature (103 °C). Compared to zLLDPE of equal crystallinity, mLLDPE is known to have much narrower distribution of lamellae thickness together with lower values of the most probable thickness [22]. On the other hand a conventional zLLDPE has broad molecular weight distribution and short chain branching distribution. The branches are preferably located in the lower molecular weight chains; thus, zLLDPE behaves as if it was a blend of higher molecular weight linear and lower molecular weight branched molecules [23]. The heterogeneous distribution of polymer chains together with the lower comonomer content of zLLDPE (5.5%) is reflected as a broad melting region at higher temperatures (127 °C).

The silica particles are known to nucleate the polymer crystallization, increasing its crystallinity, decreasing crystallite thickness, and influencing the orientation of the lamella in the crystallites [24]. At a silica content up to 4%, the increase in the melt enthalpy (crystallinity content) of the endotherm of Fig. 2—see also Table 2—together with the shifting of the crystallization temperature to higher temperatures (from 3 up to 5 °C) of the corresponding exotherm of Fig. 4 suggest that the silica nanoparticles may nucleate the mLLDPE crystallization. As can be seen from the corresponding Figs. 3 and 5 and Table 3 the nucleating role of the silica nanoparticles to the crystallization of

Table 2
DSC results for mLLDPE/SiO_2 nanocomposites

Sample type (nano-SiO_2) (wt%)	T_m (°C)	Heat of fusion (J/g)	x_c (%)	T_g (°C)
0	103.0	100.8	34.8	−40
3	101.7	114.5	39.5	−30
4	105.0	116.3	40.1	−30
6	104.0	103.5	36.7	−30
8	103.3	97.2	33.5	−40
10	103.3	84.6	29.2	−15

Table 3
DSC results for zLLDPE/SiO_2 nanocomposites

Sample type (nano-SiO_2) (wt%)	T_m (°C)	Heat of fusion (J/g)	x_c (%)	T_g (°C)
0	127.1	113.7	39.2	−50
3	125.0	119.0	41.0	−40
4	126.1	116.3	40.1	−30
6	125.8	110.3	38.0	−25
8	123.8	108.8	37.5	−25
10	126.4	103.6	35.7	−20

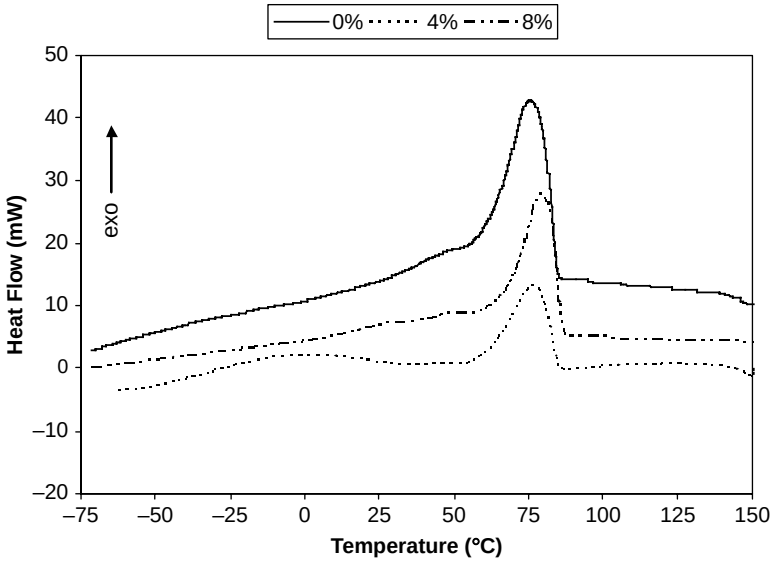

Fig. 4. DSC thermograms of non-isothermal crystallization for the mLLDPE/SiO_2 nanocomposites at a cooling rate of 20 °C/min.

zLLDPE is smaller. At a silica content of more than 4% the decrease to the crystallinity degree can be explained by the presence of an excessive number of silica particles which can hinder the motion of the polymer chain segments and thus, retard crystal growth.

The paracrystalline region in the zLLDPE/SiO_2 composites is attributed to the presence of imperfect crystals nucleated by silica nanoparticles. The size of these crystals will decrease and the corresponding 'shoulder' will shift to lower temperatures, by increasing the silica content because of the larger number of nucleation sites. Apparently, the presence of silica nanoparticles favors the separation of the linear and highly branched phases in zLLDPE. The absence of such a paracrystalline region in mLLDPE/SiO_2 composites is due probably to the overlapping with the main melting temperature (103 °C).

4.3. DMA results

The dynamic mechanical results were obtained in terms of storage modulus (E') and loss modulus (E'') and presented in Figs. 6–9. All the results associated with the various relaxation mechanisms, and their intensity are summarized in Tables 4 and 5 for mLLDPE and zLLDPE based composites, respectively. Figs. 6 and 7 show the temperature dependence of storage modulus E'. It can be observed that the storage moduli of the composites were higher than those of the corresponding LLDPE, particularly at lower temperatures, i.e. from −170 to 0 °C, while above 0 °C the differences between the various moduli became minimal. Moreover, the storage modulus E' of the composites increased with increasing the silica content and at 8% SiO_2 this trend was reversed above the

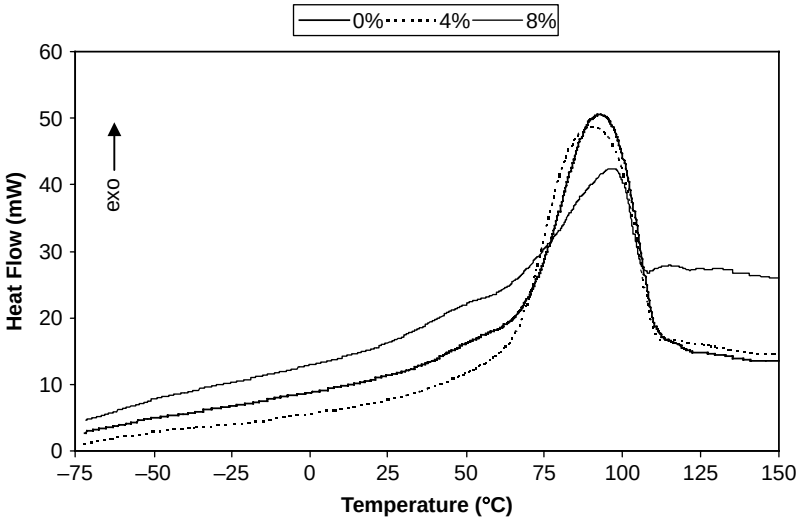

Fig. 5. DSC thermograms of non-isothermal crystallization for the zLLDPE/SiO_2 nanocomposites at a cooling rate 20 °C/min.

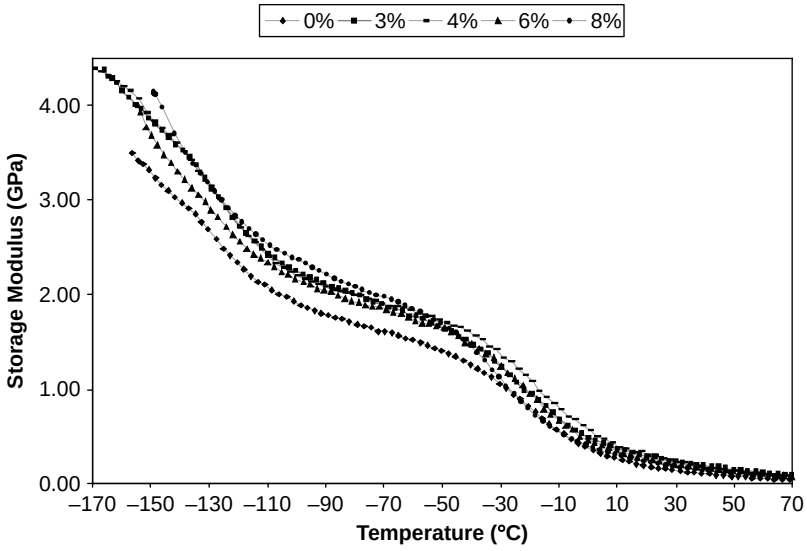

Fig. 6. Storage modulus (E') versus temperature of the mLLDPE/SiO_2 nanocomposites at a frequency of 1 Hz.

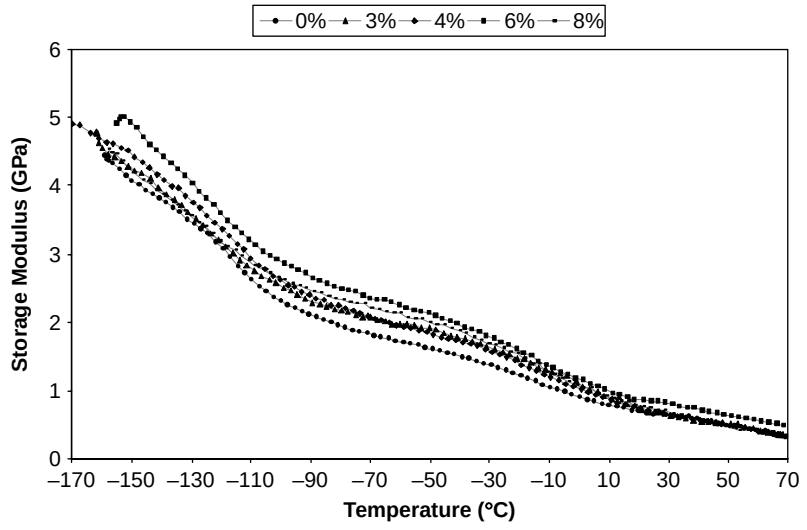

Fig. 7. Storage modulus (E') versus temperature of the zLLDPE/SiO_2 nanocomposites at a frequency of 1 Hz.

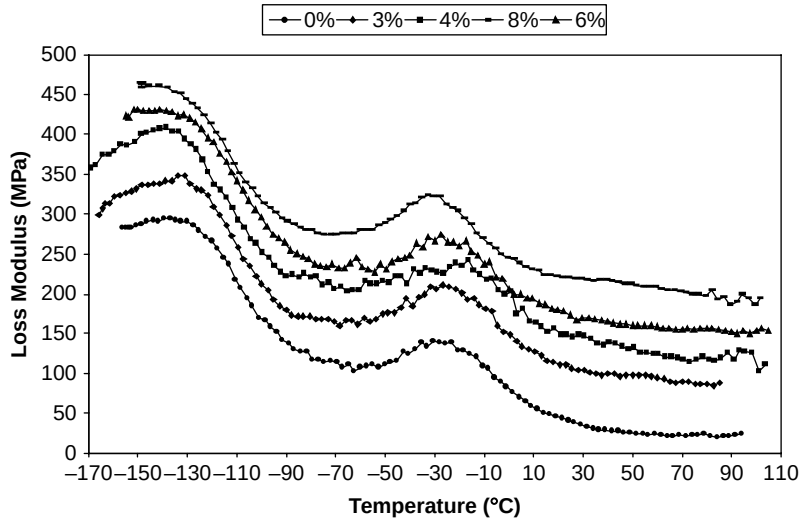

Fig. 8. Loss modulus (E'') versus temperature of the mLLDPE/SiO_2 nanocomposites at a frequency of 1 Hz. The curves have been shifted in the y-direction to make them distinguishable.

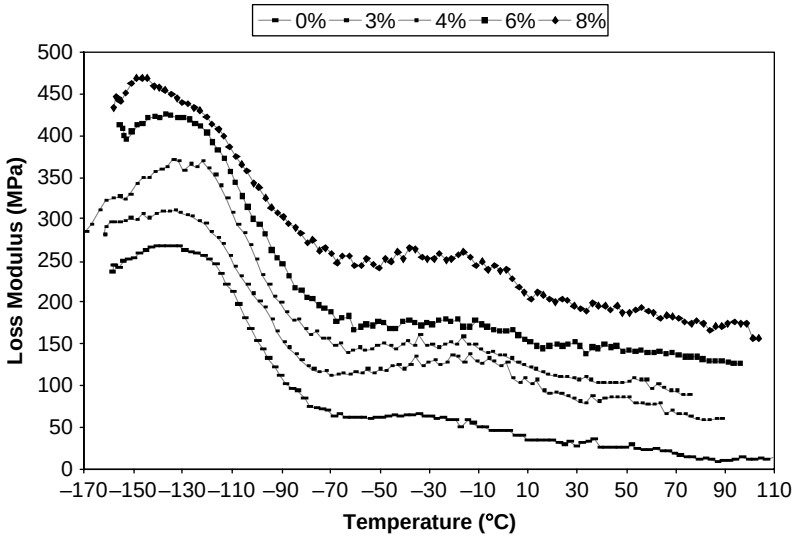

Fig. 9. Loss modulus (E'') versus temperature of the zLLDPE/SiO_2 nanocomposites at a frequency of 1 Hz. The curves have been shifted in the y-direction to make them distinguishable.

main transition temperature—around −40 °C. This phenomenon was more pronounced in mLDPE/SiO_2 than in zLLDEP/SiO_2 composites. This behavior can be explained as follows:

The matrix of the composite can be assumed that consists of two parts. One is the free part, where the state of the macromolecular chains is the same as that in the pure LLDPE. The other is the interphase. The interphase is formed by the physical or chemical adsorption of the polyethylene molecules and/or *trans*-crystallization on the filler's surface. The larger the interfacial area and the stronger the interaction between the matrix and the fillers, the greater the volume of the interphase. Because the macromolecular chains of the interphase are restricted to the surface of the fillers, the molecular motion is greatly limited. As a result, the storage modulus of the interphase is higher than that of the free part. An increase in the silica content enlarges the interfacial area and results in an increased volume of interphase. However, at higher silica content (8%) the particles tend to form extended agglomerates—see SEM micrographs of Fig. 1(b) and (d). At lower temperatures, motion of silica particles at the contact points is possible because of the high modulus of the matrix. This motion contributes significantly to the improvement of the storage modulus of the composites [25]. Composites with a silica content of 8% have a larger number of particle–particle contacts, and therefore, a higher storage modulus than the rest of the composites. At higher temperatures, the particle–particle motion largely ceased because the modulus of the free part decreased, while the storage modulus of the interphase remained unchanged. Therefore, the contribution of the interphase to the modulus of the composites is much higher at higher temperatures than at lower temperatures [7,8]. However, as a result of the aggregation of the silica particles, it is considered that the interphase of the composite with a silica content of 8% has been reduced. Therefore, above the transition temperature, the storage modulus of said composite is lower than the rest of the composites.

The reversion of the storage modulus of the 8%-nanocomposite above the main transition temperature is less pronounced in the zLLDPE/SiO_2 nanocomposite than in the mLDDPE/SiO_2 one. This is attributed to the higher modulus of the free part of the zLLDPE/SiO_2 composite (higher crystallinity).

Figs. 8 and 9 show the temperature dependence of loss modulus (E'') of the mLLDPE/SiO_2 and zLLDPE/SiO_2 composites, respectively. As can be seen also from Tables 4 and 5, the loss moduli of the composites are higher than those of the corresponding LLDPE.

All the LLDPE-based materials exhibited a γ-transition in the temperature range of −145 to −135 °C. The position of the γ-transition peak (−135 °C) was not significantly affected

Table 4
DMA results for mLLDPE/SiO_2 nanocomposites

Sample type (nano-SiO_2) (wt%)	Loss modulus (peak position) (°C)		Loss modulus (peak height) (MPa)	
	T_γ	T_β	T_γ	T_β
0	−136	−30	0.29	0.14
3	−135	−26	0.32	0.21
4	−135	−20	0.39	0.23
6	−137	−22	0.34	0.18
8	−145	−32	0.31	0.17
10	−147	−31	0.28	0.18

Table 5
DMA results for zLLDPE/SiO_2 nanocomposites

Sample type (nano-SiO_2) (wt%)	Loss modulus (peak position) (°C)		Loss modulus (peak height) (MPa)	
	T_γ	T_β	T_γ	T_β
0	−139	−40	0.32	0.12
3	−136	−28	0.33	0.16
4	−135	−29	0.27	0.17
6	−137	−31	0.30	0.11
8	−145	−37	0.39	0.17
10	−142	−22	0.40	0.16

by changes in the silica content. However, the γ-transition peak intensity increased with increase in the silica content, reaching a maximum at a silica content of 4% and then decreased. At a silica content of 8% the γ-transition shifted to −145 °C. This relaxation is attributed to the motions of the CH_2 units in the amorphous region and is independent of comonomer content [16].

Furthermore, all samples exhibited a β-transition temperature in the temperature range from −40 to −20 °C. From studies on various polyethylenes and their copolymers, this relaxation temperature has been associated with motions of chain units in the interfacial region [16]. The β-transition peak of the mLLDPE/SiO_2 nanocomposites shifted to higher temperatures with increasing the silica content and the intensity of the peak increased reaching a maximum at a silica content of 4% per weight and then this trend is reversed. This result is in contrast to other results of the prior art where the position of the β-transition peak remained unchanged [7,8]. The increase in the intensity and the shift of the location of the β-transition to a higher temperature could mean that the size of the interphase is increased up to a silica content of 4% per weight and its mobility is suppressed. At a silica content of more than 4% the decrease in the intensity and the shift of the location of the β-transition to lower temperatures could be attributed to the formation of extended agglomerates—see SEM micrographs of Fig. 1(b)—which reduce the available interfacial region. The β-transition peak of zLLDPE/SiO_2 nanocomposites was not affected by changing the filler content.

4.4. Tensile stress–strain results

The engineering stress–strain curves of mLLDPE/SiO_2 and zLLDPE/SiO_2 composites are presented in Figs. 10(a) and 11(a), respectively. Corresponding Figs. 10(b) and 11(b) focus in the low strain range. The tensile properties of all materials tested are presented in detail, in Tables 6 and 7. With respect to macroscopic behavior during the tensile tests, all samples showed neck formation and plastic flow.

As can be seen in Fig. 10(a) and (b) and Table 4, for the mLLDPE/SiO_2 nanocomposites examined, a general increment in elastic modulus, and yield stress is obtained, with increasing the filler content. The addition of the nanofillers brings up also an increase in the tensile strength of mLLDPE accompanied by

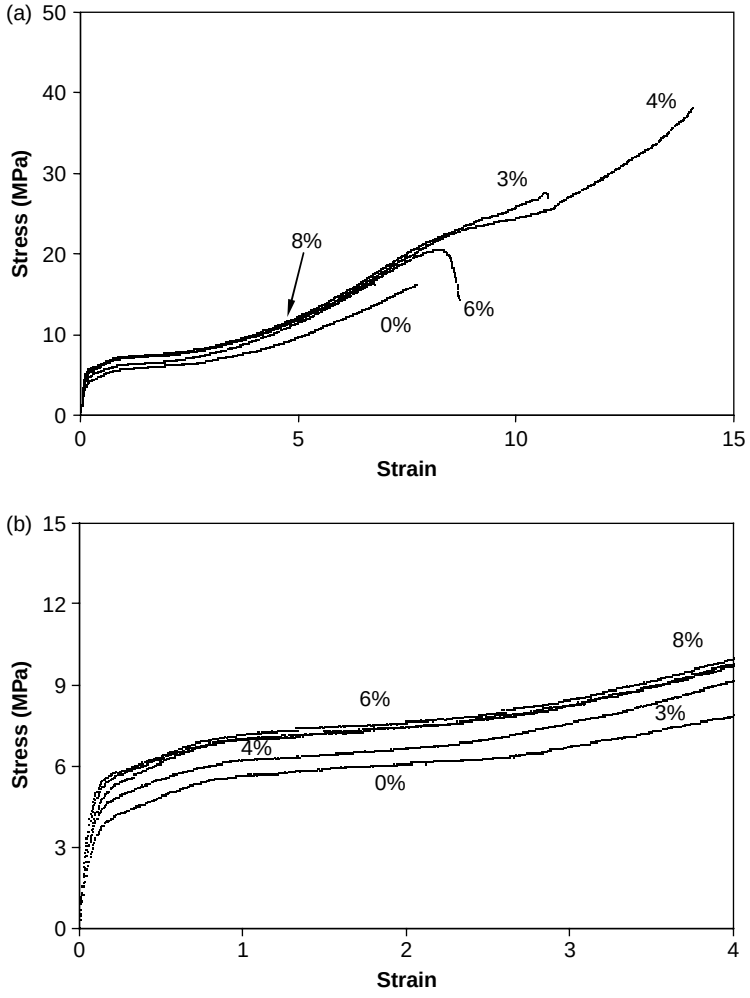

Fig. 10. (a) Tensile stress–strain curves of the mLLDPE/SiO_2 nanocomposites at a strain rate of $5.55\times10^{-3}\,s^{-1}$. (b) Tensile stress–strain curves of the mLLDPE/SiO_2 nanocomposites in the low strain range.

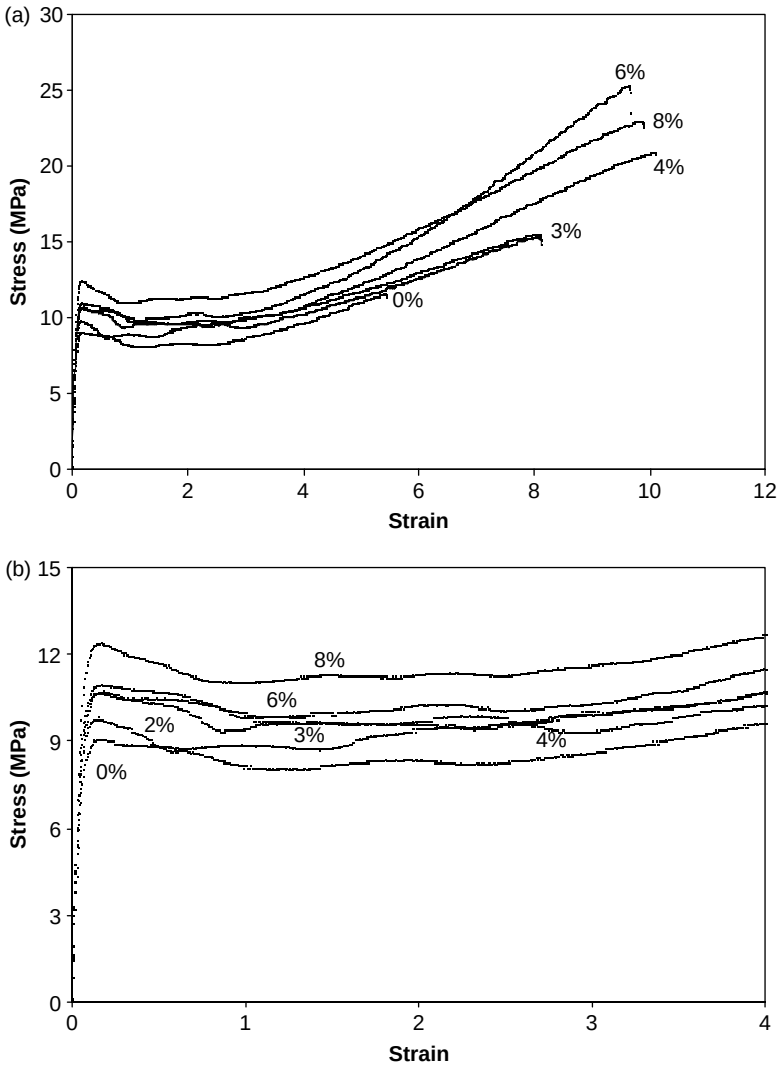

Fig. 11. (a) Tensile stress–strain curves of the zLLDPE/SiO_2 nanocomposites at a strain rate of 5.55×10^{-3} s^{-1}. (b) Tensile stress–strain curves of the zLLDPE/SiO_2 nanocomposites in the low strain range.

a significant increase in the elongation at break. The same trend, although to a lesser extent, was observed in Fig. 11(a) and (b) and Table 7 for the zLLDPE/SiO_2 composites.

As is shown in Fig. 10(b) the mLLDPE-based materials exhibit double yield point (although the second yield point is less pronounced), which are inflection points. The appearance of a double yield point has been reported for low crystalline ethylene copolymers and branched polyethylenes under tension [26–28]. The first yield point occurs at low strain and marks the onset of temporary plastic deformation, the second yield point occurs at higher strains, marks the onset of permanent plastic deformation, and is associated with the development of a neck in tension. The yield-morphology relationships are complicated. Among other factors, crystallinity and crystallite size are viewed as most important [27–29]. The double yield form with the two inflection points of mLLDPE is attributed to the smaller size and the narrower distribution of the crystallites as result of the higher

Table 6
Tensile Properties for mLLDPE/SiO_2 nanocomposites

Sample type (nano-SiO_2) (wt%)	Elastic modulus (MPa)	Yield stress (MPa)	Strain at break	E_c/E_m
0	51	3.7	7.8	1
3	55	4.2	10.8	1.23
4	70	5	14.0	1.36
6	82.0	5.4	8.3	1.61
8	103	5.5	11.0	2.03
10	65	7.2	9.0	1.28

Table 7
Tensile Properties for zLLDPE/SiO_2 nanocomposites

Sample type (nano-SiO_2) (wt%)	Elastic modulus (MPa)	Yield stress (MPa)	Strain at break	E_c/E_m
0	230	10.5	5.5	1
3	237	11.0	8.1	1.03
4	240	9.0	10.0	1.04
6	245	11.0	9.5	1.07
8	280	12.9	9.6	1.22
10	153	10.8	9.0	0.66

comonomer content (15%) of mLLDPE and its polymerization method (metallocene). On the other hand, as is shown in Fig. 11(a), the zLLDPE-based materials show sharp yield points, which are local yield maxima, followed by a strain softening, which render them unsuitable as stretch films. This behavior can be attributed to the broad distribution of crystal thickness. As can be seen in Tables 6 and 7, for the weight percentage of nanofiller used, the yield stress did not change significantly when compared to the pure LLDPEs.

The tensile properties of the LLDPE/SiO_2 nanocomposites indicate that the silica nanoparticles stiffen and toughen LLDPE. At a silica content of 4% per weight, optimal properties were obtained in elastic modulus, tensile yield strength, tensile strength and elongation at break. At a nanoparticle content equal to or higher than 8% per weight the mechanical properties of the nanocomposites start to deteriorate. The observed changes in the tensile properties cannot be due to changes in crystallinity and is more likely to be due to the presence of the inorganic inclusions, especially at higher silica content.

The mechanical behavior of LLDPE/SiO_2 nanocomposites could be explained as follows

Generally, the elastic modulus increases with augmenting filler content, while all other tensile properties, such as the yield stress and strain, tensile strength and elongation at break almost invariably decrease with increasing filler content [11].

Nanoparticles and polymer chains have comparable time scales for motion because of their size similarity. Due to their mobility, the nanoparticles can act as temporary crosslinks between the polymer chains, providing localized regions of enhanced strength, which in turn can retard the growth of cracks or cavities. Similarly, energy dissipation might be further enhanced due to the presence of smaller and hence more mobile crystallites [30]. An efficient nanoscale dispersion coupled with favorable polymer–silicate interactions is critical for improved toughness. At a silica content of 8% the nanoparticles form extended agglomerates, as can be seen in the SEM micrographs of Fig. 1(b) and (d), which weaken the interfacial adhesion, reduce the number of debonding/voiding sites and decrease the toughness of the nanocomposites.

5. Micromechanics models

Along with the improved chemical and physical properties of nanocomposites, the mechanical properties such as stiffness, strength and toughness have been studied due to their great potential in engineering. There is a large number of works dealing with material synthesis and characterization of polymer nanocomposites, but the fundamental mechanisms for mechanical property improvement are not yet completely defined [31–34]. Assuming that the polyethylene-nanocomposites studied in this work are composed of a continuous isotropic matrix and discrete isotropic spherical inhomogeneities, the overall stiffness tensor of this system will be calculated. The estimation of the stiffness tensor will be based on previous works by Taya and Chou [35] and Chen and Cheng [36]. Their works deal with the effective moduli of composites containing misoriented fibers and both are based on the Eshelby [37] and Mori–Tanaka [38] theory. Chen et al have extensively studied the effective elastic moduli of planar orientation distribution and transversely isotropic distribution of fibers. The interaction among fibers at different orientations was included in their analysis by adopting the mean stress concept of Mori–Tanaka together with eigenstrain idea of Eshelby. The prediction of the effective moduli of fiber-reinforced thermoplastics (FRTP) was then possible. By extending this analysis, they have calculated the effective moduli tensor for spherical particles, acting as reinforcing agents. On the other hand, Taya and Chou [35] starting from the same concept of Eshelby and Mori–Tanaka theory, have proceed to the calculation of the longitudinal effective modulus of composite materials, including two different types of inclusions, such as two fiber types with different aspect ratios and stiffness, or a combination of fiber and particles. In their work also the analysis can be reduced in the case of particulate reinforcement.

5.1. The effective moduli tensor

When an infinite elastic body is subjected to a uniform stress-field $\boldsymbol{\sigma}_0$ the corresponding uniform strain $\boldsymbol{\varepsilon}_0$ is:

$$\boldsymbol{\varepsilon}_0 = \mathbf{C}_m^{-1} \cdot \boldsymbol{\sigma}_0 \tag{1}$$

where $\mathbf{C}_m$ is the elastic modulus tensor of the isotropic matrix. When there are ellipsoidal inclusions present in the matrix, a perturbed stress field is induced. Then the average stress field into the matrix is given by:

$$\boldsymbol{\sigma}_m = \boldsymbol{\sigma}_0 + \bar{\boldsymbol{\sigma}} = \mathbf{C}_m \cdot (\boldsymbol{\varepsilon}_0 + \bar{\boldsymbol{\varepsilon}}) \tag{2}$$

where $\bar{\boldsymbol{\sigma}}$ is the volumetric average of the perturbed stress field, and $\bar{\boldsymbol{\varepsilon}}$ is the perturbed strain field. If all inhomogeneities are aligned in one direction, according to Taya and Mura [39], and the fact that the disturbed stress must be zero when it is integrated in the total volume, the following two expressions are extracted:

$$\mathbf{C}_m[\bar{\boldsymbol{\varepsilon}} + f_1(\boldsymbol{\varepsilon}^{pt} - \boldsymbol{\varepsilon}^*)] = 0 \tag{3}$$

$$\boldsymbol{\sigma}_f = \mathbf{C}_f \cdot \boldsymbol{\varepsilon}_f = \mathbf{C}_f \cdot (\boldsymbol{\varepsilon}_0 + \bar{\boldsymbol{\varepsilon}} + \boldsymbol{\varepsilon}^{pt}) = \mathbf{C}_m \cdot (\boldsymbol{\varepsilon}_0 + \bar{\boldsymbol{\varepsilon}} + \boldsymbol{\varepsilon}^{pt} - \boldsymbol{\varepsilon}^*) \tag{4}$$

where f_1 is the filler volume fraction, $\mathbf{C}_f$ is the stiffness moduli of the filler, $\boldsymbol{\sigma}_f$ the strain related with the filler, $\boldsymbol{\varepsilon}^{pt}$ is the perturbed strain and $\boldsymbol{\varepsilon}^*$ the equivalent transformation strain. The last two quantities following Eshelby [37] are related by the following equation:

$$\boldsymbol{\varepsilon}^{pt} = \mathbf{S} \cdot \boldsymbol{\varepsilon}^* \tag{5}$$

where $\mathbf{S}$ is the Eshelby tensor.

Further, in their work Chen and Cheng [36] made the assumption of a total volumetric average strain $\boldsymbol{\varepsilon}^T$ of the composite material that is given by:

$$\boldsymbol{\varepsilon}^T = f_0(\boldsymbol{\varepsilon}_0 + \bar{\boldsymbol{\varepsilon}}) + f_1(\boldsymbol{\varepsilon}_0 + \bar{\boldsymbol{\varepsilon}} + \boldsymbol{\varepsilon}^{pt}) = \boldsymbol{\varepsilon}_0 + f_1 \boldsymbol{\varepsilon}^* \tag{6}$$

where f_0 is the matrix volume fraction.

Expression (6) can alternatively be written as [36]:

$$\boldsymbol{\varepsilon}^{\mathrm{T}} = (\mathbf{I} + f_1\mathbf{B}\cdot(\mathbf{I} + f_1\mathbf{E})^{-1})\cdot\boldsymbol{\varepsilon}_0 \tag{7}$$

where

$$\mathbf{B} = \mathbf{A}\cdot\mathbf{T} \tag{8}$$

$$\mathbf{A} = \mathbf{I} - \mathbf{C}_{\mathrm{m}}^{-1}\cdot\mathbf{C}_{\mathrm{f}}$$

and

$$\mathbf{T} = (\mathbf{I} + \mathbf{S}\cdot\mathbf{C}_{\mathrm{m}}^{-1}\cdot\mathbf{C}_{\mathrm{f}} - \mathbf{S})^{-1}$$

$$\mathbf{E} = (\mathbf{S} - \mathbf{I})\cdot\mathbf{A}\cdot\mathbf{T}$$

The effective moduli tensor $\mathbf{C}^*$ of the composite will thus be given by:

$$\boldsymbol{\sigma}_0 = \mathbf{C}^*\cdot\boldsymbol{\varepsilon}^{\mathrm{T}} \tag{9}$$

Finally from Eqs. (1), (8), (9) $\mathbf{C}^*$ will be given by:

$$\mathbf{C}^* = \mathbf{C}_{\mathrm{m}}\cdot\left[\mathbf{I} + f_1\mathbf{B}\cdot(\mathbf{I} + f_1\mathbf{E})^{-1}\right]^{-1} \tag{10}$$

where $\mathbf{I}$ is the identity matrix tensor.

On the other hand, Taya and Chou [35] starting from analogous expressions regarding the stress and strain field, and using the concept of the eigenstrain by Eshelby [37], have considered the interactions among inclusions, introducing the idea of a 'back stress'. They have calculated the overall stiffness of a hybrid composite, which includes two kinds of inhomogeneities. In their work, the longitudinal modulus was calculated by using the equivalence of the strain energies and is given by the expression:

$$\frac{E_\ell}{E_0} = \frac{1}{1+\eta} \tag{11}$$

where E_ℓ is the longitudinal modulus of the composite material and E_0 is the matrix elastic modulus. The quantity η is a complicated function of the filler volume fraction, the elastic constants of the filler and matrix, as well as the components of the Eshelby tensor. This function is analytically presented in the work of Taya and Chou [35].

In both above-mentioned cases, the Eshelby tensor components for spherical inclusions are:

$$S_{11} = S_{22} = S_{33} = \frac{7-5\nu_0}{15(1-\nu_0)} \tag{12}$$

$$S_{12} = S_{23} = S_{31} = -\frac{1-5\nu_0}{15(1-\nu_0)}$$

$$S_{44} = S_{55} = S_{66} = \frac{4-5\nu_0}{15(1-\nu_0)}$$

where ν_0 is the Poisson ratio of the matrix.

In Fig. 12 the normalized modulus of the composites in respect to the matrix modulus (E_c/E_m) is plotted versus filler volume fraction f_1, and compared to the theoretical predictions. From this figure, a different stiffness enhancement for the two composite types is observed. mLLDPE-based composites exhibit a much higher relative modulus compared to the zLLDPE-based composites. The increase in tensile modulus together with a concurrent increase in tensile strength and elongation at break is a strong evidence of a better toughness–stiffness balance [40]. As is shown in Fig. 12, the zLLDPE/SiO_2 composites follow Eq. (10) with a good accuracy. The normalized modulus of mLLDPE/SiO_2 composites increases with nanofiller loading but at a higher rate than that predicted by Eq. (11). In both models a perfect adhesion between filler and matrix has been assumed and this might be the main reason for the high deviation between experimental and theoretical results for the mLLDPE composites. In any case, the above results indicate the limitations of the conventional models when applied to nanocomposites.

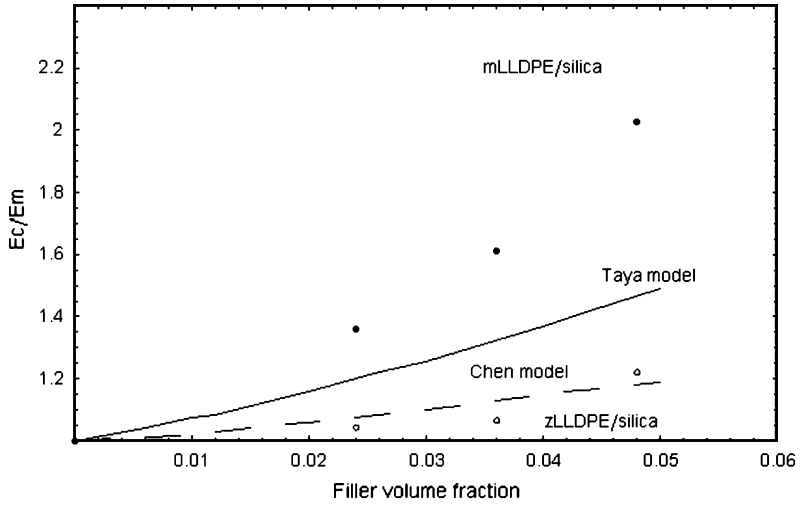

Fig. 12. Normalized modulus (E_c/E_m) versus filler volume fraction (f_1). The continuous and broken lines represent the Taya and Chen models, respectively. The dark and white circles represent the experimental values of the mLLDPE/SiO_2 and zLLDPE/SiO_2, respectively.

In conventional composites reinforced with inorganic fillers, the size of the dispersed particles is of the order of micrometers and the interfacial region is often not taken into account [41]. When the dispersed particles have a size in the nano-scale, the surface area of the dispersed phase becomes very large, resulting in an increase in the volume of interfacial region, which may be comparable with that of the dispersed phase. It has been shown that for nanometer-sized reinforcement, the molecular structure of the polymer matrix is significantly perturbed at the matrix-filler interface and this perturbed region is on a length scale that is the same as that of the dispersed particle [42].

Additionally, the radius of gyration of macromolecules and the interface width of incompatible polymer systems are of this order of magnitude. The macromolecular segments which are adsorbed on the nanofiller's surface would be less mobile than those in the bulk matrix. Therefore, the finer the dispersed phase or the thicker interfacial region results in a higher tensile modulus for the composite materials. This effect appears to be dominant for the mLLDPE composites, and it may be related to the uniform distribution of molar mass or distribution of the crystalline blocks among amorphous regions.

In a recent work by Odegard et al. [43] an elastic micromechanics model was developed for silica nanoparticle/polyimide composites with various nanoparticle/polyimide interfacial treatments. This model includes an effective interface between the matrix and the nanoparticles with properties and dimensions, which are determined using the results of molecular dynamics simulations. The effective interface has a finite size and models the region surrounding the spherical reinforcement, which is commonly referred to as an interphase.

According to this micromechanics model [43,44], the elastic stiffness tensor is given by:

$$\mathbf{C} = \mathbf{C}_0 + [(f_1 + f_i)(\mathbf{C}_i - \mathbf{C}_0)\mathbf{T}_i + f_1(\mathbf{C}_f - \mathbf{C}_i)\mathbf{T}_f] [f_0\mathbf{I} + (f_1 + f_i)\mathbf{T}_i]^{-1} \quad (13)$$

where f_i is the interface volume fraction, $\mathbf{C}_i$ is the inteface stiffness tensor, and $\mathbf{T}_f$, $\mathbf{T}_i$ are some strain concentration tensors given by:

$$\mathbf{T}_f = \mathbf{I} - \mathbf{S}[\mathbf{S} + (\mathbf{C}_f - \mathbf{C}_0)^{-1}\mathbf{C}_0]^{-1} \quad (14)$$

$$\mathbf{T}_i = \mathbf{I} - \mathbf{S}\left\{\frac{f_1}{f_i + f_1}[\mathbf{S} + (\mathbf{C}_f - \mathbf{C}_0)^{-1}\mathbf{C}_0]^{-1} + \frac{f_i}{f_i + f_1}[\mathbf{S} + (\mathbf{C}_i - \mathbf{C}_0)^{-1}\mathbf{C}_0]^{-1}\right\}$$

where $\mathbf{S}$ is the Eshelby tensor [37], whose components appear in Eq. (12) for particles as a dispersed phase. It is obvious from Eq. (13) that the composite stiffness tensor is isotropic for spherical particle reinforcement. The effective interface model should be applicable to both nanometer sized and larger-sized reinforcement.

As is shown in Fig. 13, the effective interface model, as expressed by Eq. (13), approximates adequately the experimental behavior of mLLDPE. For the best fitting of the experimental data, the volume fraction of the interface was assumed to be equal to the half of the matrix volume fraction. This is an assumption close to the results of molecular modeling, performed in the work by Odegard et al. [43]. This is also consistent with the fact that nanocomposites differ from conventional microcomposites because of their larger interfacial area per unit volume and the smaller interparticle distance. The presence of many chains at the interphase means that much of the polymer is 'interphase-like' [32].

The effective interface was also assumed to be continuous, homogeneous and isotropic, requiring two independent elastic constants to define $\mathbf{C_i}$. Its Poisson ratio was taken equal to 0.33, the same with the polymer matrix. The elastic modulus was taken equal to 2.4 GPa. This value is also close to the corresponding value in the work by Odegard et al. [43], where the dispersed phase is similar to that applied in our work. Following the above mentioned assumptions, the normalized modulus of the mLLDPE/SiO_2 in respect to the matrix

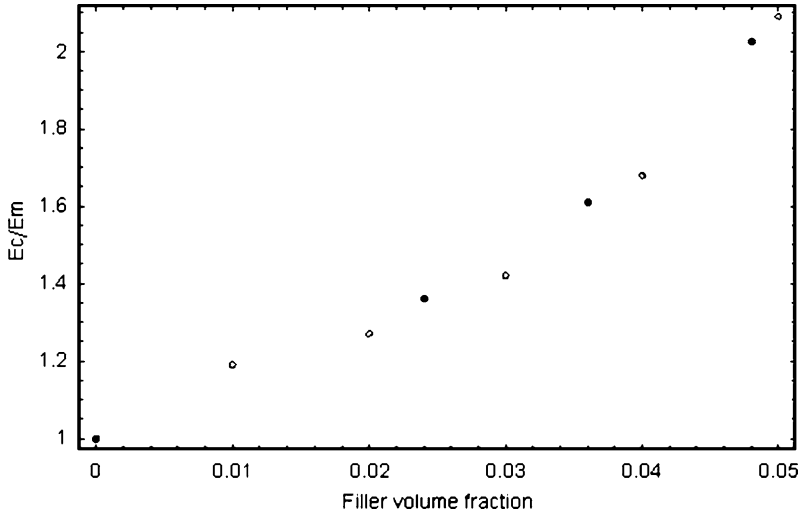

Fig. 13. Normalized modulus (E_c/E_m) versus filler volume fraction (f_1) of the mLLDPE/SiO_2 composites. Dark circles represent the experimental values. The white circles represent the theoretical values calculated according to the interface model (Eq. (13)).

modulus, is plotted versus filler volume fraction, in comparison with the theoretical data obtained applying the interface model, expressed by Eq. (13).

6. Conclusions

The previous experimental results indicated that only a small amount of surface-modified nano-silica particles can effectively improve modulus, yield, strength, toughness and thermal deformation temperature of LLDPE. Such an improvement in overall properties of polymers can scarcely be observed in conventional microparticulate composites. The optimum silica content is ~4% per weight for the nanocomposites studied. This can bring substantial improvement to the savings of the composites. In general, over 20% of micron-sized particles are required to achieve a similar performance. Higher silica content brings no significant improvement to the properties, while adds to the cost of the composite. Silica contents above 8% are detrimental to the properties of the composites.

The thermo-mechanical properties of the mLLDPE/SiO_2 composites are affected to a greater extent by changes in the silica content, than the corresponding mLLDPE/SiO_2 composites, possibly because of their lower crystallinity content.

The addition of the nanofillers brought up an increase in the elastic modulus and the tensile strength of mLLDPE accompanied by a significant increase in the elongation at break. The same trend, although to a lesser extent, was observed for the zLLDPE/SiO_2 composites. The increment of the elastic modulus of the composites with increasing filler weight fraction was simulated with three micromechanical models developed in previous works. The model that assumes an effective interface between the matrix and the nanoparticles provided the best fitting with the experimental data of mLLDPE/SiO_2

It can be concluded that nanofillers, as opposed to the conventional micrometer-size fillers, do not only increase the stiffness of the polymer, but also by modifying morphology, as well by introducing new energy-dissipation mechanisms, enhance the toughness of the nanocomposites.

References

[1] Wu CS. J Polym Sci, Part A 2005;43(8):1690–701.
[2] Liao HT, Wu CS. J Polym Sci, Part B 2004;42(23):4272–80.
[3] Zhang F, Li S, Karaki T, Adachi M. Jpn J Appl Phys, Part 1: Regul Pap Short 2005;44(1):658–61.
[4] (a) Alexandre M, Dubois P, Sun T, Garces JM, Jerôme R. Polymer 2002; 43(8):2123–32.
(b) Alexandre M, Dubois P, Sun T, Garces JM, Jerôme R. Note Rev Pap 2005;44(1):658–61.
[5] Wang KH, Koo CH, Chung IJ. J Appl Polym Sci 2003;89:2131–6.
[6] Hotta S, Paul DR. Polymer 2004;45(22):7639–54.
[7] Huang YQ, Jiang S, Libo W, Hua YQ. Polym Test 2004;23(1):9–15.
[8] Hunag YQ, Zhang YQ, Hua YQ. J Mater Sci Lett 2003;22(14): 997–8.
[9] Hua YQ, Zhang YQ, Wu LB, Huang YQ, Wang GQ. J Macromol Sci, Part B Phys 2005;44(2):149–59.
[10] Zhang MQ, Rong MN, Zhang HB, Friedrich K. Polym Eng Sci 2003; 43(2):490–500.
[11] Osman MA, Rupp JEP, Suter UW. Polymer 2005;46:1653–60.
[12] Truss RW. J Mater Sci Technol 2005;21(1):101–3.
[13] Lazzeri A, Zebarjad SM, Pracella M, Cavalier K, Rosa R. Polymer 2005; 46(3):827–44.
[14] Alexandre M, Dubois P. Mater Sci Eng 2000;28:1–63.
[15] Kelarakis A, Yoon K, Sics I, Somani RH, Hsiao BS, Chu B. Polymer 2005;46:5103–17.
[16] Niaounakis M, Kontou E. J Polym Sci, Part B: Polym Phys 2005;43: 1712–27.
[17] Guth E. J Appl Phys 1945;16:20–5.
[18] Kerner EH. Proc Phys Soc 1956;B69:808.
[19] Brady JM, Thomas EL. J Pol Sci, Part B: Polym Phys 1988;26:2385.
[20] Wu CL, Zhang MQ, Rong MZ, Friedrich K. Compos Sci Technol 2002; 62:1327–40.
[21] Bikiaris DN, Vassiliou A, Pavlidou E, Karayannidis P. Eur Polym J 2005; 41:1965–78.
[22] Gaucher-Miri V, Elkoun S, Seguela R. Polym Eng Sci 1997;37(10): 1672–83.
[23] Prasad A. Polym Eng Sci 1998;8(10):1716–28.
[24] Bartczak Z, Argon AS, Cohen RE, Kowalewski T. Polymer 1999;40: 2367–80.
[25] Lee BL, Nielsen LE. J Polym Sci, Phys Ed 1977;15:683–92.
[26] Balsamo V, Müller AJ. J Mat Sci Lett 1993;12(18):1457–9.
[27] Seguela R, Darras O. Mater Sci 1994;29(20):5342–52.
[28] Brooks NWJ, Duckett RA, Ward IM. J Polym Sci, Part B: Polym Phys 1998;36(12):2177–89.
[29] Lucas JC, Failla MD, Smith FL, Mandelkern L, Peacock A. J Polym Eng Sci 1995;35(13):1117–23.
[30] Shah D, Maiti P, Gunn E, Schmidt DF, Jiang DD, Batt CA, et al. Adv Mater 2004;16(14):1173–7.
[31] Wang J, Pyrz R. Compos Sci Technol 2004;64:925–34.
[32] Brune DA, Biccerano J. Polymer 2002;43:369–87.
[33] Lincoln DM, Vaia RA, Wang ZG, Hsiao BS. Polymer 2001;42: 1621–31.
[34] Shelley JS, Mather PT, De Vries KL. Polymer 2001;42:5849–58.
[35] Taya M, Chou T-W. Int J Solids Struct 1981;17:553–63.
[36] Chen C-H, Cheng C-H. Int J Solids Struct 1996;33(17):2519–39.
[37] Eshelby JD. Proc R Soc London 1957;A241:376–96.
[38] Mori T, Tanaka K. Acta Metall 1973;21:571–4.
[39] Taya M, Mura T. ASME J Appl Mech 1981;48:361.
[40] Motha K, Hippi U, Hakala K, Peltonen M, Ojanperä V, Löfgren B, et al. J Appl Polym Sci 2004;94:1094.
[41] Xiang Ling JL, Jiao KJ, Wei Jiang, Zheng J. Polym Eng Sci 2002;42(5): 983–93.
[42] Odegard GM, Gates TS, Wise KE, Park C, Siochi E. Compos Sci Technol 2003;63(11):1671–87.
[43] Odegard GM, Clancy TC, Gates TS. Polymer 2005;46:553–62.
[44] Dunn ML, Ledbetter H. J Appl Mesh 1995;62(4):1023–8.